COMPRESSION CORNER SHOCK WAVE BOUNDARY LAYER INTERACTIONS AT MACH 14

G. Simeonides and J.F. Wendt
von Karman Institute for Fluid Dynamics
B-1640 Rhode Saint Genèse-Belgium

Abstract

New pressure and heat transfer measurements over a flat plate / 2D compression ramp configuration at Mach 14 are presented. The measurements were carried out in the VKI Longshot heavy piston gun tunnel at unit Reynolds numbers in the range 6 to 13 million per meter. The wind tunnel, test conditions, and model configurations are described; emphasis is placed on the quality of the measurements. The measured pressure and heat transfer distributions in the transitional interaction zones resulting from the deflection of the ramp at 15° and 25° are compared to simple analytic prediction methods and a Navier-Stokes computation. The capability to predict peak heating rates in the region of reattachment and the limitations of simple correlations are discussed. Streamwise striations were observed in this region to cause large spanwise variations in the heat transfer rate and to promote transition of the reattaching boundary layer. This heating variation was found to be bounded by the laminar and turbulent attached heating levels, which were well predicted by simple flat-plate boundary layer theory.

LIST OF SYMBOLS

C	Chapman-Rubesin constant, $\frac{\mu T_e}{\mu_e T}$
c_{DN}	leading edge drag coefficient
c_f	skin friction coefficient
d	leading edge thickness
K_e	$\equiv M_\infty^3 c_{DN} \frac{\gamma-1}{\gamma+1} \frac{d}{x}$
K_p	pressure coefficient = $\frac{p-p_\infty}{\frac{1}{2}p_\infty M_\infty^2}$
M	Mach number
p	pressure
Re	Reynolds number
St	Stanton number
T	temperature
u	velocity
x	distance from leading edge
x_3	distance from virtual origin of reattaching boundary layer
γ	ratio of specific heats
μ	viscosity
ξ	distance from nozzle exit
$\overline{\chi}$	hypersonic viscous interaction parameter

Subscripts

0	reservoir
1	upstream of interaction (inviscid)
3	downstream of reattachment (inviscid)
∞	freestream
b	due to bluntness
e	edge of boundary layer
inf	freestream
L	at hinge line
mod	modified
p	plateau
perf	equivalent perfect gas
pk	peak
r	recovery (adiabatic wall)
real	real gas
ref	reference
t_2	stagnation point
u	upstream of interaction (viscous)
v	due to viscous interaction
w	wall

Superscript

*	at Eckert's reference temperature

1. INTRODUCTION

Shock wave boundary layer interactions have been the subject of extensive research. Since the phenomenon was first observed by Ferri in 1939, a large number of configurations at various conditions have been investigated, but still many questions remain unanswered. In addition, most investigations have focused on applications to missile aerodynamics and have thus been concerned with high Reynolds numbers and consequently turbulent boundary layers at supersonic Mach numbers.

The recent boost in space transportation technology characterized by a number of ambitious projects worldwide (Hermes, Sänger, Hotol, NASP) has been accompanied by increased interest in fundamental research directly related to ascent/reentry aerodynamics. Focusing on reentry and particularly on its initial stages, the associated aerodynamics are characterized by high Mach numbers (M>10 to 15) and relatively low unit Reynolds numbers (high altitude); consequently, fully laminar boundary layers are expected to develop on various wetted surfaces.

Referring to figure 1, attention is drawn to control surfaces such as the body flaps, elevons and rudders on the wing-tip fins. Upon deflection of these control surfaces, severe shock wave boundary layer interactions are anticipated (largely enhanced by the laminar character of the oncoming boundary layers) which will result in loss of control effectiveness and high heating rates. It need be stressed that such interactions will be directed by strong three dimensional effects resulting from the finite span and the sweep of the control surfaces as well as the three dimensionality of the incoming flow.

Extensive reviews of shock wave boundary layer interactions may be found in [1-4]. The present study concen-

trates on the problem of the deflected control surface which is simulated by a 2D or swept ramp placed some distance along a flat plate (Fig. 2). Experiments have so far been carried out with a flat plate/2D ramp model in the von Karman Institute's Longshot facility at Mach 14 with the ramp deflected at 0°, 15°, and 25° with unit Reynolds numbers in the range 6.5×10^6 to 13×10^6 per meter.

The experimental program is outlined in section 2, followed by a preliminary analysis of results in section 3 with emphasis on the quality of results, repeatability, flow establishment time and finite span effects. Sections 4 and 5 present the results of the parametric study, namely the effects of Reynolds number and ramp angle and comparisons of the measurements to simple flat plate theory and a Navier-Stokes computation performed by Haase [5]. A discussion on striation heating in the region of reattachment is also included.

2. EXPERIMENTAL PROGRAM

2.1 The Longshot wind tunnel

A schematic of the Longshot facility [6,7] is shown in figure 3. It is a free-piston gun tunnel, comprising a driver chamber (initially pressurized with nitrogen gas to 300 atm and ambient temperature) and a driven tube (initially pressurized with dry nitrogen to just over 1 atm at ambient temperature), the two being separated by a heavy piston weighing from 1.8 to 5 kg. The piston is supported at its initial position by an aluminum diaphragm. Bursting of this diaphragm results in the acceleration of the piston into the driven tube and the compression of the dry nitrogen test gas into a reservoir volume at the downstream end of the driven tube. Pressures as high as 4000 bar and temperatures to 2500 K may be attained in the reservoir. The compressed test gas is trapped in the reservoir (about 320 cm^3) by the automatic closure of 48 poppet valves. The subsequent bursting of a secondary copper diaphragm upstream of the throat of the contoured hypersonic nozzle allows the test gas to expand to Mach 14 into the test section. The nozzle exit diameter is 42.7 cm with a uniform test core of 24 cm. Due to the finite reservoir volume, the duration of a test is limited to 15-20 ms, and the flow conditions continuously decay during the test time.

To completely define the test conditions, assuming isentropic flow, one needs a measure of the reservoir pressure, reservoir temperature, and pitot pressure in the test section. The reservoir and pitot pressures are directly measured, whereas the reservoir temperature is extracted through an iterative procedure based on the Fay-Riddell theory [8] from the heat transfer rate measured at the stagnation point of a sphere in the test section (Fig. 4). Due to the high reservoir pressure and temperature, dense gas effects and vibrational excitation must be taken into account [9]. The test conditions are calculated with an uncertainty shown in Fig. 5.

The variation of the measured reservoir pressure and the calculated reservoir temperature with time is shown in figure 6. The reservoir pressure decays exponentially, the characteristic time τ of this decay being about 9 ms. In addition, data are considered only for times greater than the leftmost boundary of figure 6a (i.e., about 1 ms after the peak conditions) in order to avoid inaccuracies related to the response characteristics of transducers in the region of sharp time-gradients of the signals. The rightmost boundary in figure 6a indicates the end of the useful running time, as this is dictated by the onset of condensation of the test gas in the test section, predicted by the Daum & Gyarmathy semi-empirical theory [10]. Although Mach number remains nominally constant with time, Reynolds number decays during a test as illustrated in figure 6c.

An illustration of the uniformity of the flow in the test section is given in figure 7, where the transverse pitot pressure distribution is plotted across the test core of 24 cm at two axial stations, 20 mm and 250 mm from the nozzle exit. Most of the variation of the pitot pressure at a given axial station falls within the uncertainty band of pitot pressure measurements, whereas an acceleration along the test section is observed corresponding to a Mach number increase of 1.5% over a length of 250 mm from the nozzle exit.

2.2 Models

The model configuration is illustrated in figure 2 in the test section of the wind tunnel. It comprises a forward flat plate, 200 mm in length, with a sharp leading edge, and a rear plate, 200 mm in length configured at 0°, 15° or 25° to the forward part. A schematic of the model with the 15° ramp is shown in figure 8. The model span is 200 mm.

In fact, two similar model configurations have been used in this study. One was equipped with both pressure and heat transfer instrumentation, the other solely with heat transfer gauges.

The former model was instrumented between 66 and 380 mm from the leading edge along the centerline, and the gauges were spaced at 10 mm intervals. The flat plate part had only pressure instrumentation, whereas on the ramp alternating pressure and heat transfer gauges were installed. At 146 mm from the leading edge, pressure instrumentation was installed at 20 mm and 40 mm off the centerline, and for the 15° ramp, at 290 mm from the leading edge at 30 mm and 50 mm off the centerline. Also, at 290 mm from the leading edge on the 15° ramp, five heat transfer gauges were installed spanwise at 2 mm intervals from the centerline. The thickness of the leading edge of this model varied from 58μm at the centerline to 52 μm near the edges. No significant change of the leading edge was observed during the tests.

The second model was instrumented solely with heat transfer gauges along the centerline between 100 mm and 305 mm from the leading edge. They were spaced at 4 mm intervals on the flat plate part and 5 mm on the ramp. The leading edge thickness of this model was 35 μm $\pm$ 10μm.

Finally, experiments were carried out with and without side plates which are also illustrated in figure 8. The side plates covered the entire interaction region for both the 15° and 25° ramp.

2.3 Instrumentation and data reduction

Due to the short duration of tests in the Longshot tun-

nel, individual pressure transducers have been employed at each pressure measuring port. The transducers are normally installed into an L-shaped probe to protect them from any particulate matter present in the flowfield. This configuration exhibits a probe/transducer response time of a fraction of a millisecond.

The pressure transducers employed are Endevco 8514-20 and Endevco 8507-15 with respective full scales of 20 and 15 psi; their diameters are 1.65 mm and 2.34 mm, respectively. They are used with a vacuum reference pressure and are statically calibrated before each test. Their typical output signal is 5 bar/volt.

Five Kulite XCQ-X-080-100 absolute pressure transducers were also employed, kindly loaned to the VKI by the RWTH Stosswellenlabor, Aachen. The full scale of these transducers is 100 psi and they have a 2.03 mm diameter.

For heat transfer measurements, the semi-infinite slab principle was employed [11], in which the transient surface temperature rise was measured by thin film resistance thermometers placed on a MACOR * substrate on the flat plate part of the model and by coaxial thermocouples manufactured by the Medtherm Corporation and installed in X17-U4 steel inserts on the ramp.

Data acquisition is accomplished by a dedicated 16-bit system of 64 sets of amplifiers, filters and transient recorders with a maximum acquisition frequency capability of 50 kHz per channel, controlled by a personal computer. The measurement chain also includes 32 wheatstone bridge circuits for use with pressure transducers, 48 constant current circuits for use with thin film gauges and 24 differential amplifiers for use with coaxial thermocouples.

Results are presented in coefficient form. The pressure coefficient is defined as

$$K_p = \frac{p - p_\infty}{\frac{1}{2}\gamma p_\infty M_\infty^2}$$

and a modified Stanton number defined as

$$St_{mod} = \frac{\dot{q}_s}{\rho_\infty u_\infty c_p (T_{0_{perf}} - T_w)}$$

2.4 Test matrix

The bulk of the data is presented for M_∞=14.1, T_∞ = 58.5K and Re_{unit}=6.5×10^6 and 9.1×10^6 per meter. The test conditions in all tests were repeatable within their uncertainty bands. The model temperature was 295K. In total, fifteen tests were carried out at the low Reynolds number condition (6.5×10^6/m) and eleven tests at the medium Reynolds number condition (9.1×10^6 /m). One test was also carried out with the 25° ramp at Re_{unit}=13×10^6/m to further study the influence of Reynolds number. The freestream temperature for this test was also 58.5K but the Mach number was 14.6.

* MACOR:machinable ceramic manufactured by Corning Inc.

It was noted in section 2.1 that the test conditions decay with time. The data presented herein are instantaneous data within the useful running time (Fig. 6) for the corresponding instantaneous test conditions. This procedure assumes a quasi-steady flow behaviour which will be justified in the following section.

3. QUALITY OF RESULTS

3.1 Accuracy of measurements

Error analysis has yielded an uncertainty for the raw measurements of ±15% for pressure on the flat plate part of the model, ±2.5% for (higher) pressure levels on the ramp and ±7% for heat transfer measurements (both on the flat plate measured by thin film gauges and on the ramp measured by the less sensitive coaxial thermocouples). The resulting uncertainty levels are : for the pressure coefficient, ±17% on the flat plate and ±4.5% on the ramp, and ±25% for the Stanton number.

3.2 Repeatability and finite span effects

The repeatability of pressure measurements is illustrated in figure 9. With reference to figure 9a and, noting that test 909 incorporated side plates, finite span effects for the 15° ramp test case are judged to be small as they cause only a minor increase in the streamwise extent of the interaction. It is seen in figure 9b, however, that finite span effects are far more pronounced in the 25° ramp test case. It is noted that in both cases spanwise pressure measurements taken at 146 mm from the leading edge (within the separated zone) do not show any significant spanwise pressure variation; it is stressed that this is a necessary but not sufficient condition for two-dimensionality. The repeatability of heat transfer measurements is illustrated in figure 10. It is noted that the large variation observed at 290 mm from the leading edge in figure 10a is not scatter but corresponds to a spanwise variation of the heat transfer rate indicating the presence of streamwise striations. This topic will be discussed in section 5.3.

3.3 Flow establishment time

Holden has studied [2,12] the time required for flow establishment in a well-separated flow region, and concluded that, once the flow in the wind tunnel is established, the establishment of the separated region is well described by the time required for an acoustic disturbance travelling at the wall speed of sound to traverse the steady separation length. As opposed to base flow separations, acoustic propagation time dominates viscous mixing time. Holden found [12] that for the case of a 2D separated flow the edge boundary condition along the model sides does not influence the flow establishment time. This, however, contradicts the findings of Rudy et al. [13] where a 3D time-accurate computation for Holden's 2D flat plate/compression ramp experiments converged to a steady state solution considerably faster than the corresponding 2D computation.

For the present Longshot experiments a maximum separation length of 0.15 m has been observed which from Holden's criterion would require about 0.5 ms to become established. Since data are examined at times greater than 1 ms after peak tunnel conditions and the hypersonic flow has already established by the time of peak conditions, flow

establishment problems are not expected to be encountered in the ramp tests considered herein.

This conclusion is supported by the time-dependent pressure measurements carried out in and outside of the interaction region, illustrated in figure 11. Examination of the pressure coefficient-time traces of figure 11 indicates that only gauge number 3 passes from an attached flow regime into a separated regime within the useful running time. This phenomenon is not seen in any of the other gauges, including the one immediately downstream (gauge 4), and is a result of a small increase in the scale of separation with the decaying reservoir conditions during the test, rather than a result of establishing flow. It is noted that the above results show that the establishment time of the separated region is small compared to the characteristic time of change of the test conditions, and so data may be considered, at any instant of time, as quasi-steady.

4. ANALYSIS OF PRESSURE MEASUREMENTS

4.1 Flat plate

The data presented herein are characterized by a hypersonic viscous interaction parameter, $\overline{\chi}$, ranging between 1 and 4. For a cold wall (T_w/T_0=0.12) this implies a weak viscous interaction over the flat plate, for which the analysis in [14] yields

$$\frac{p_v}{p_\infty} - 1 = 0.115\overline{\chi}$$

In addition, the pressure distribution over the flat plate will be influenced by the blunt leading edge of the pressure model. This effect may be approximated by the zero order inviscid theory of [15] which, for a strong leading edge effect, yields

$$\frac{p_b}{p_\infty} = 0.5342K_e^{2/3}$$

Following the discussion in [14, 15], the combined viscous and inviscid effects may be approximated by the sum of the two partial effects. This result is compared to the measurements in figure 12 and results in an underprediction of about 25%. It should be noted, however, that for the present test conditions, the leading edge effect is also weak and a higher order theory is necessary to accurately predict it. Finally, it is noted that the direct comparison of the measurements to the above prediction assumes zero pressure gradient across the hypersonic boundary layer which may be another cause for the observed discrepancy.

4.2 Ramp cases

A schlieren photograph for the 15° ramp case is shown in figure 13. Separation, S, is seen to occur at about 140 mm from the leading edge and reattachment, R, at about 250 mm from the leading edge, close to the impingement point, I, of the separation shock. The deflection, D, of the free shear layer upstream of reattachment is also noted, as well as the transitional/turbulent nature of the reattaching boundary layer.

The effect of Reynolds number on the pressure distribution along the centerline of the 15° and 25° ramp configurations is shown in figures 14a and 14b, respectively. A plateau pressure is observed just downstream of separation, followed by a sharp rise to a peak value and a subsequent decay to the inviscid pressure level [16]. Increasing Reynolds number is seen to cause a mild reduction in the extent of separation which indicates that the present interactions are transitional, this being consistent with the schlieren observations. Also, with reference to figure 11, the pressure near the separation point is seen to increase with time, that is with decreasing Reynolds number, which is also an indication of a transitional interaction after the criterion developed in [17].

Also shown in figure 14 is the result of a correlation presented in [2] for the plateau pressure in laminar interactions as,

$$\frac{p_p - p_u}{p_u} = \overline{\chi}_L^{3/8}$$

which is based on the concept of free interaction.

Using the measured values for p_u, very good agreement is found with the measured plateau pressure, despite the transitional nature of the interaction. In fact, although the turbulent level of plateau pressure is expected to be considerably higher than the laminar level [4], it is pointed out in [17] that the difference between a laminar and a transitional interaction will be small.

Finally, a comparison between the measured pressure distribution and the Navier-Stokes computation of [18] is shown in figure 15. Also, the weak viscous interaction result for the flat plate is shown. It is noted that both the Navier-Stokes and flat plate computations underpredict the measured flat plate pressure levels as expected, since both neglect the leading edge effect. Consequently, the Navier-Stokes computation underpredicts the plateau pressure, as it takes a lower upstream pressure level; reasonably good agreement is found with the plateau pressure correlation of [2] provided only the viscous interaction component of p_u is taken into account.

In general, very good agreement is found between measurements and the Navier-Stokes computation of [18] including the streamwise extent of separation. The inviscid pressure level on the ramp is also indicated after [16]. Both experiment and computation show a pronounced peak in the pressure level near reattachment which is explained by the processing of the flow near the wall through a double shock system (separation and reattachment shocks, figure 13)[19]. The inviscid analysis in [19] also points out that the expansion fan caused by the intersection of the two shocks may yield wall pressure levels downstream of the peak which are lower than the inviscid single shock values of [16]. In fact, this is an effect seen in the laminar calculation of [18].

5. ANALYSIS OF HEAT TRANSFER MEASUREMENTS

5.1 Flat plate

The Stanton number distribution along the flat plate configuration is plotted against Reynolds number in figure 16. It is compared to a reference temperature prediction method based on the Blasius solution for the incompressible skin friction coefficient [20] and Reynolds analogy in the

form

$$St = \frac{c_f}{2Pr^{2/3}}.$$

Eckert's definition of reference temperature [21] is employed. The justification for using a zero pressure gradient technique for the prediction of the heat transfer distribution lies in the argument of [14] that for a cold wall the pressure gradient term in the momentum equation is small and so its effect may be neglected. The result is

$$St_{mod,e} = \frac{0.41}{\sqrt{Re_{e,x}}}\sqrt{C_e^*}\left(\frac{T_r - T_w}{T_{0_{perf}} - T_w}\right)$$

where

$$C_e^* = \frac{\mu^* T_e}{\mu_e T^*}$$

and

$$T_e^* = T_e + 0.5(T_w - T_e) + 0.22(T_r - T_e)$$

It is noted that this result employs local boundary layer edge properties, which, due to the viscous interaction and leading edge effects, differ from the freestream properties. Therefore,

$$St_{mod} = St_{mod,\infty}$$

$$= \left(\frac{p_e u_e}{p_\infty u_\infty}\right)^{1/2} \frac{0.41}{\sqrt{Re_{\infty,x}}}\sqrt{C_\infty^*}\left(\frac{T_r - T_w}{T_{0_{perf}} - T_w}\right)$$

In the implementation of this equation, the measured pressure along the flat plate has been used, after scaling of the leading edge bluntness contribution to the thinner leading edge of the heat transfer model. This scaling was done according to the law $p_b/p_\infty \propto K_e^{2/3}$. For illustration purposes, the curve obtained on the assumption that the boundary layer edge conditions are the same as in the freestream is also shown. Both results are in reasonable agreement with the experimental data.

5.2 Global heat transfer distributions on the ramp configurations

The effet of Reynolds number on the heat transfer distribution along the 15° and 25° ramp configurations is illustrated in figures 17a and 17b, respectively. For the 25° ramp model, the first heat transfer gauge was just downstream of separation. With reference to figure 17a, upstream of the interaction the flat plate values are measured and the expected $\sqrt{Re_{\infty,x}}$ dependence for a laminar attached boundary layer is seen. The most pronounced effect of Reynolds number is observed in the reattachment region on the 15° ramp. Whereas in all 25° ramp cases a clear peak in Stanton number is observed in the reattachment region, this peak is less pronounced in the 15° ramp cases, especially so in the lower Reynolds number condition. Noting that reattachment in all cases is transitional/turbulent, the effect is attributed to the dependence of the location and extent of transition on Reynolds number. To be sure, if transition is occurring at the location of minimum thickness of the reattaching boundary layer, then the continuous rise from the laminar to the turbulent attached heating levels may override the decay of heating rate as the boundary layer thickness increases downstream and yield a less pronounced peak.

The effect of ramp angle is illustrated in figure 18 for the lower Reynolds number case. Also shown is the laminar flat plate prediction discussed in section 5.1. A similar solution, but for a turbulent boundary layer, is compared to the heat transfer distribution along the two ramps. The conditions downstream of the inviscid shock [16] have been used as edge conditions, and a virtual origin of the reattaching boundary layer at 240 mm from the leading edge has been assumed. The expression for the turbulent skin friction coefficient comes from [20, 22] and the result is

$$St_{mod,turb} = \frac{0.0368}{Re_{\infty,x_3}^{1/5}}\left(\frac{T_\infty}{T^*}\right)^{4/5}\left(\frac{\mu^*}{\mu_\infty}\right)^{1/5}\left(\frac{p_3 u_3}{p_\infty u_\infty}\right)^{4/5}$$

Surprisingly good agreement is found between the measurements and this simple flat plate solution. There exists, however, the problem of defining the virtual origin of the reattaching boundary layer and its relative location to the point of peak heating (i.e., the neck of the boundary layer downstream of reattachment) if an accurate estimate for the latter is to be obtained.

In fact, the above analysis forms the backbone of correlations developed for peak heating in shock wave boundary layer interactions [22,23] in the form

$$\frac{h_{pk}}{h_{ref}} = \left[\frac{p_3}{p_1}\right]^n \quad \text{or} \quad \left[\frac{p_{pk}}{p_1}\right]^n$$

Still, for the above relation to be strictly valid, h_{ref} must be defined from the same virtual origin as the reattaching boundary layer; however, normally, h_{ref} is defined from the leading edge or nose of the model, in which case the above correlation should incorporate a constant of proportionality which is a function of $(x_{3pk}/x_{pk})^n$ or, in other words, of the thinning of the boundary layer aft of reattachment. This may partly explain the wide scatter of data exhibited in such correlations and the wide variety of exponents found in the literature as summarized in [23].

To conclude this section, a comparison between the measured Stanton number distribution and the Navier - Stokes computation of [18] for the lower Reynolds number 15° ramp case is shown in figure 19. Also shown are the laminar and turbulent reference temperature predictions for the ramp, and the laminar reference temperature prediction for the flat plate. The former assume an origin for the boundary layer at the leading edge and also at 240 mm from the leading edge to illustrate the effect of the choice of the virtual origin of the reattaching boundary layer. The latter, in this case, has been obtained using only the viscous interaction component of the flat plate pressure field, in order to compare to the Navier-Stokes computation which neglects the leading edge effect. Indeed, the weak viscous interaction theory is in good agreement with the Navier-Stokes solution and they both slightly underpredict the flat plate heating level. Again, the Navier-Stokes solution of [18] is found in very good agreement with the measurements and it supports the conjecture that transition, in this test case, is occurring very near reattachment.

5.3 Striation heating

It was pointed out in section 3.2 that the spanwise heat transfer variation observed at 290 mm from the leading edge in figure 10a is evidence for the presence of streamwise striations in the region of reattachment. These striations have been observed in a variety of supersonic/hypersonic reattaching flows [4,17,24,25], as illustrated in figure 20. The phenomenon is described as an instability in the 2D flow and attributed to the formation of streamwise Görtler vortices [24, 26] due to the streamwise curvature near reattachment. The formation of Görtler vortices, in turn, has a destabilizing effect and provides a mechanism for transition [17, 24]. The spanwise variation in heat transfer in such flow situations has been measured to be as much as ±50% [17].

The limited spanwise heat transfer measurements performed in the present series of experiments just downstream of reattachment on the 15° ramp are plotted as a percentage variation along the span in figure 21. Also shown are infrared [25] and thin film measurements taken along the span of the 15° ramp model just aft of reattachment in the conical Mach 15 nozzle of the Longshot tunnel with Re_{unit} = 14×10^6/m. The amplitude of the infrared measurements has been corrected for the limited spatial resolution of the infrared scanning radiometer [25,27].

The striation pattern in figure 21 is evident and characterized by a spatial period of approximately 8 mm, as expected from the findings of [17] which noted that the wavelength of the streamwise vortices is between 2 and 3 times the undisturbed boundary layer thickness. The measured spanwise heat transfer variation is up to ±35% whereas the present experiments have shown a variation of ±15 to 20%. However, noting the spanwise period of these striations, the present spacing and finite size of thermocouples has not been sufficient to fully resolve the resulting variations and has been used only as an indicator of the presence and effect of striations.

Finally, it is noted that all present measurements fall below the local turbulent heating level, as can be seen in figure 19. In fact, even a ±50% spanwise variation in Stanton number would place the heating distribution between the laminar and fully turbulent levels. This observation supports the view that streamwise striations form a mechanism for transition which, in turn, may explain why a majority of laminar separated flows are found to be transitional/turbulent at reattachment.

6. CONCLUSIONS

New pressure and heat transfer measurements performed at Mach 14 in the VKI Longshot heavy piston gun tunnel over a flat plate/2D compression ramp configuration have been presented together with a discussion on the quality of results.

Measurements over the flat plate/15° and 25° ramp configurations have been compared to simple analytical prediction methods and correlations as well as to the Navier-Stokes computations of Haase and, generally, good agreement was found.

The weak viscous interaction and the weak leading edge bluntness effects were found to be significant for the pressure distribution over the flat plate but not so for the heat transfer distribution which was well predicted by a zero pressure gradient reference temperature method.

Severe shock wave/boundary layer interactions were found to occur upon deflection of the ramp to 15° and 25° resulting in significant separated regions. Although the oncoming boundary layer was laminar, the reattachment process was found to promote transition in all cases and to yield turbulent peak heating rates. This transition process was related to the observed streamwise striations developing in the region of reattachment which may yield large heating variations between the laminar and turbulent levels along the span of the ramp.

Noting the sharp pressure rise just downstream of the hinge line to a peak value higher than the inviscid levels, the loss of control effectiveness due to the shock wave boundary layer interaction should, in general, not pose a major design constraint. The most important effect of the interaction is the promotion of transition at reattachment and the associated high turbulent heating levels. It was found that the reference temperature flat plate theory performed well in predicting heating rates at reattachment, although it requires knowledge of the degree of thinning of the boundary layer in the neck region in order to accurately predict peak heating rates.

Finally, the Navier-Stokes computations of Haase compare favorably with the experimental data supporting the view that transition is promoted by the reattachment process. They have demonstrated the need to incorporate in the computations a transition model near reattachment, although for engineering calculations turbulent attached flow predictions may suffice to provide an upper limit on the heating rate.

Acknowledgement

This research was partially supported by Avions Marcel Dassault-Bréguet Aviation under the terms of the Hermes R&D program RD MFE 2/87. The technical monitor was Mr. P. Perrier.

REFERENCES

1. Green, J.E.: Interactions between shock waves and turbulent boundary layers. *Progress in Aerospace Sciences*, Vol. 11, 1970
2. Hankey, W.L. & Holden, M.S.: Two dimensional shock wave boundary layer interactions in high speed flows. *AGARDograph* 203, June 1975
3. Settles, G.S. & Dolling, D.S.: Swept shock wave boundary layer interactions. in "*Tactical Missile Aerodynamics*", M.J. Hemsch & J.N. Nielsen, eds; AIAA Progress in Aeronautics & Astronautics, Vol. 104, 1986
4. Delery, J.: Shock/shock and shock wave/boundary layer interactions in hypersonic flows. *AGARD Report* 761, June 1989

5. Haase, W.: Viscous hypersonic flows over compression ramps. in Proc. 8th GAMM Conf. on *Numerical Methods in Fluid Mechanics*, ed. P. Wesseling, 1990
6. Richards, B.E. & Enkenhus, K.R.: Hypersonic testing in the VKI Longshot free piston tunnel. *AIAA Paper* 69-333
7. Simeonides, G.: The performance of the VKI Longshot hypersonic wind tunnel. *von Karman Institute TN* 161, June 1987
8. Fay, J.A. & Riddell, F.R.: Theory of stagnation point heat transfer in dissociated air. *J. Aero. Sc.*, Vol. 25, No 2, Feb 1958, pp 73-85
9. Culotta, S. & Richards, B.E.: Methods for determining conditions in real nitrogen expanding flows. *von Karman Institute TN* 58, Feb 1970
10. Daum, F.L. & Gyarmathy, G.: Condensation of air and nitrogen in hypersonic wind tunnels. *AIAA J.*, Vol. 6, No 3, March 1968
11. Schultz, D.L. & Jones, T.V.: Heat transfer measurements in short duration facilities. *AGARDograph* 165, Feb 1973
12. Holden, M.S.: Boundary layer displacement and leading edge bluntness effects on attached and separated laminar boundary layers in a compression corner. Part II-Experimental study. *AIAA J.*, Vol. 9, No 1, Jan 1971
13. Rudy, D.H., et al.: A validation study of four Navier-Stokes codes for high speed flows. *AIAA Paper* 89-1838
14. Hayes, W.D. & Probstein, R.F.: *Hypersonic flow theory.* Academic Press, 1959
15. Cheng, H.K., et al.: Boundary layer displacement and leading edge bluntness effects in high temperature hypersonic flow. *J. Aerospace Sc.*, Vol. 28, No 5, May 1961, pp 353-381
16. Equations, tables and charts for compressible flow. *NACA TR* 1135, 1953
17. Ginoux, J.J.: On some properties of reattaching laminar and transitional high speed flows. *von Karman Institute TN* 53, Sept 1969
18. Haase, W.: CFD contribution to problem 3 : flow over a 2D ramp. Workshop on *Hypersonic Flows for Reentry Problems*, Antibes, France, Jan 1990 (proceedings to be published by Springer Verlag early 1991)
19. Sullivan, P.A.: Hypersonic flow over slender double wedges. *AIAA J.*, Vol. 1, No 8, Aug 1963
20. Anderson, J.D.: *Hypersonic and high temperature gas dynamics.* McGraw Hill, 1989
21. Eckert, E.R.G.: Engineering relations of friction and heat transfer to surfaces in high velocity flow. *J. Aero. Sc.*, Vol. 22, No 8, Aug 1955, pp 585-587
22. Newman, R.D. & Hayes, J.R.: Introduction to aerodynamic heating analysis of supersonic missiles. in "*Tactical Missile Aerodynamics*", M.J. Hemsch & J.N. Nielsen, eds; AIAA Progress in Aeronautics and Astronautics, Vol. 104, 1986
23. Hung, F.T.: Interference heating due to shock wave impingement on laminar boundary layers. *AIAA Paper* 73-678
24. Kipp, H.W. & Helms, V.T.: Some observations on the occurrence of striation heating. *AIAA Paper* 85-324
25. Simeonides, G., et al.: Infrared thermography in blow-down and intermittent hypersonic facilities. *AIAA Paper* 89-0042
26. Schlichting, H.: *Boundary layer theory.* McGraw Hill, 4th ed., 1960
27. Wendt, J.F.: Infrared thermography. *Second Joint Europe/US Short Course on Hypersonics*, Colorado Springs, Jan 1989

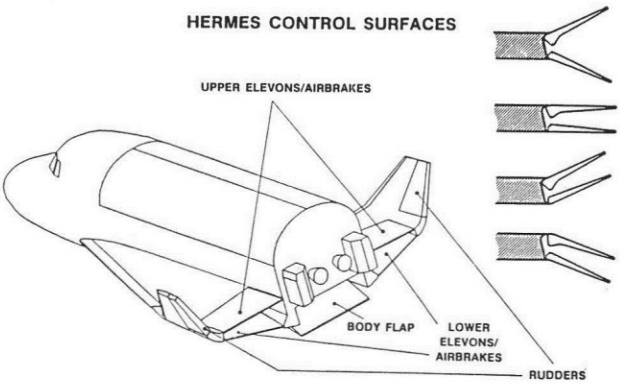

Fig. 1 - Areas of shock wave/boundary layer interactions on the Hermes reentry vehicle

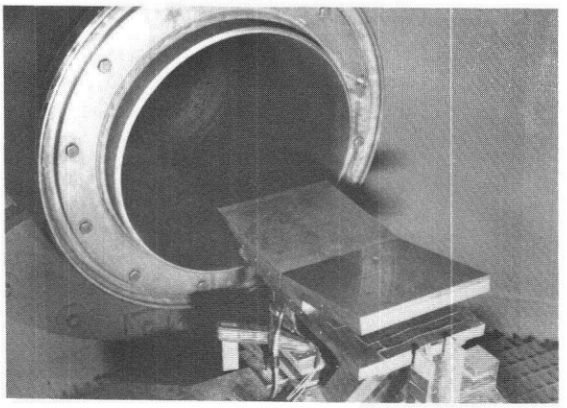

Fig. 2 - Flat plate /2D 15° ramp model

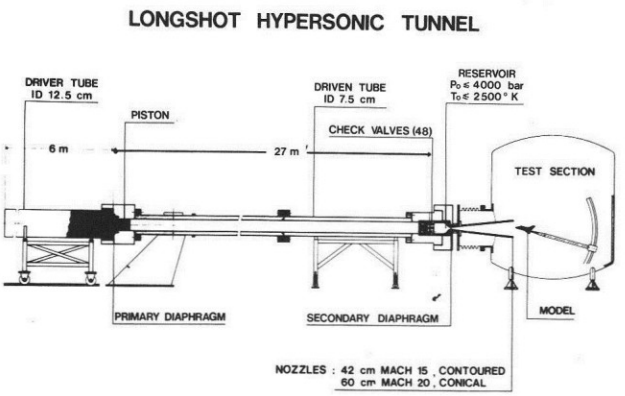

Fig. 3 - The VKI Longshot wind tunnel

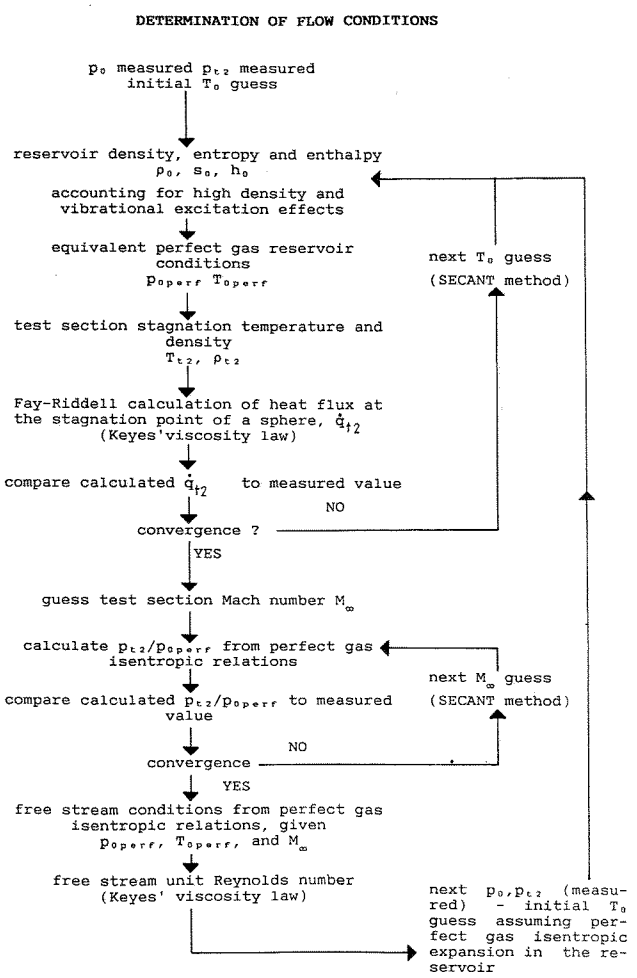

Fig. 4 - Flow chart for the determination of the Longshot test conditions

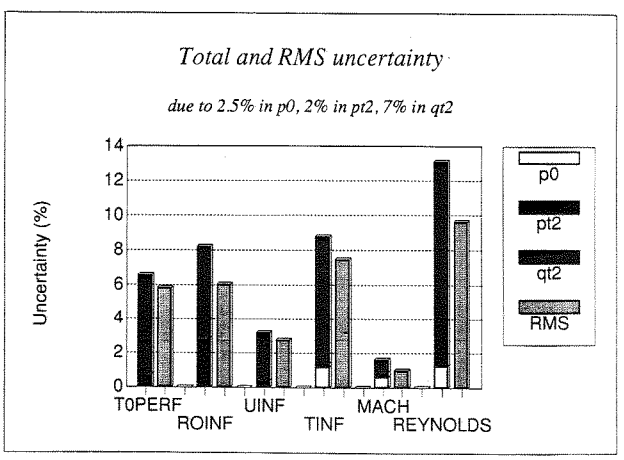

Fig. 5 - Uncertainty of test conditions in the Longshot wind tunnel

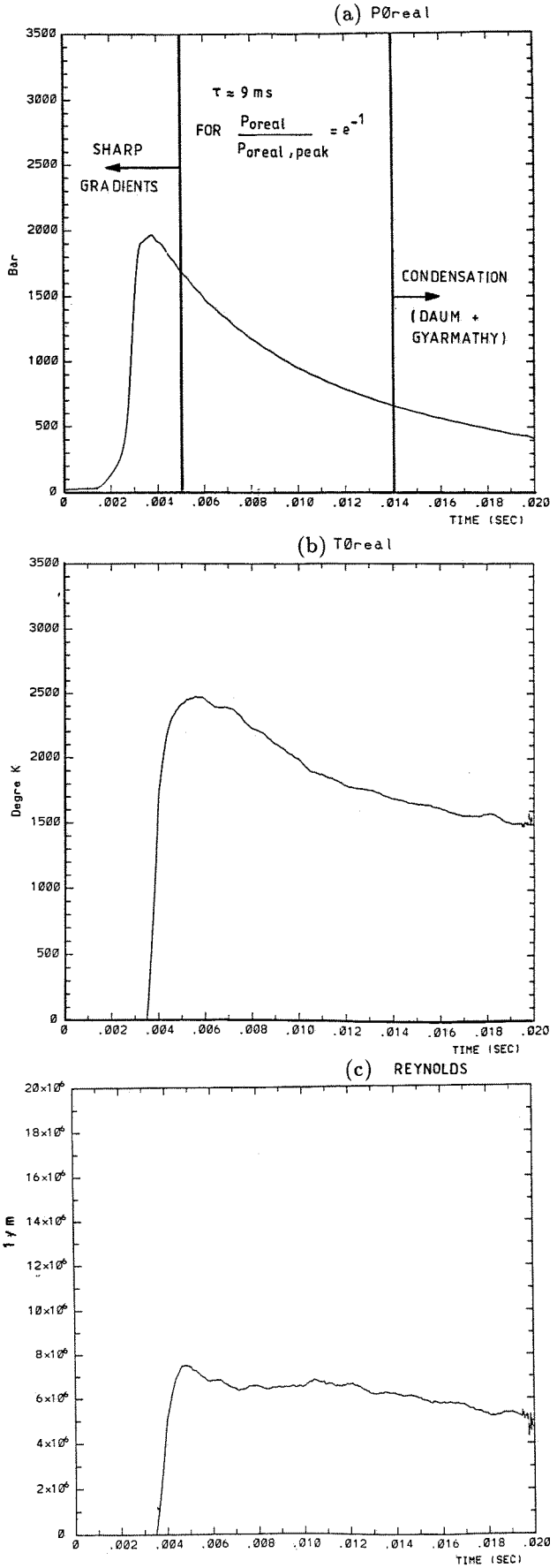

Fig. 6 - The variation of pressure and temperature in the Longshot reservoir and of the freestream unit Reynolds number

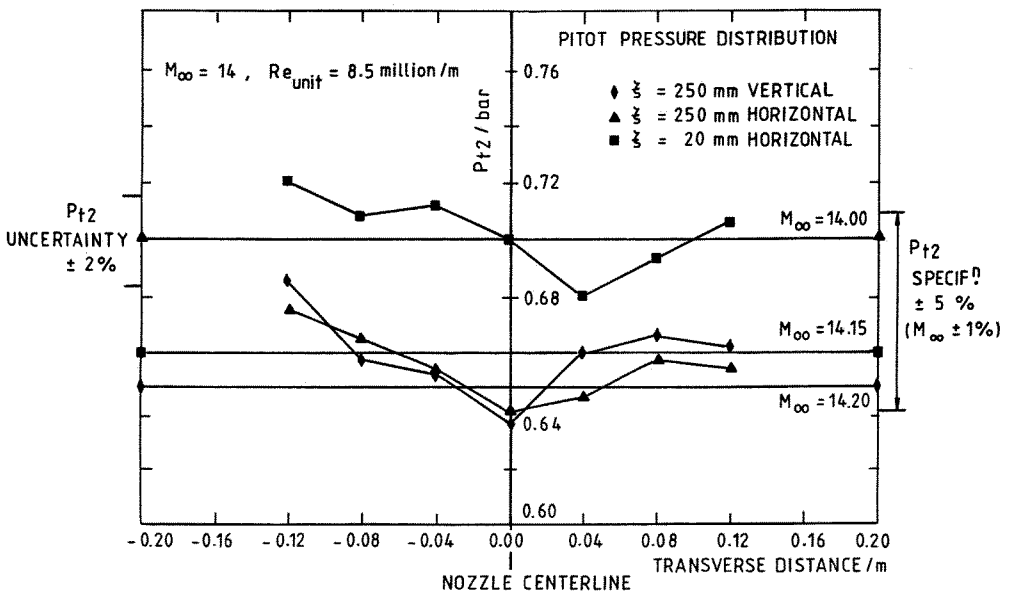

Fig. 7 - Transverse pitot pressure distributions in the Long-shot test section

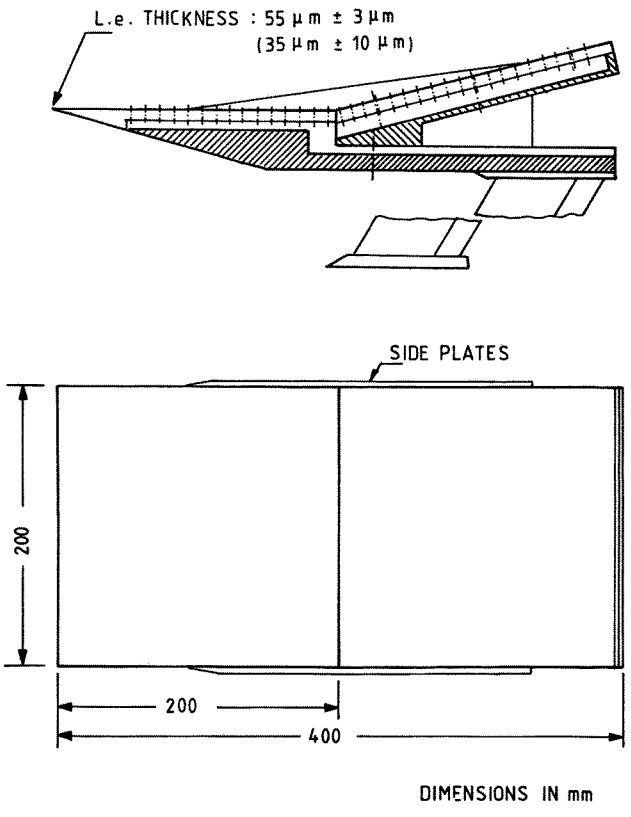

Fig. 8 - Model schematic

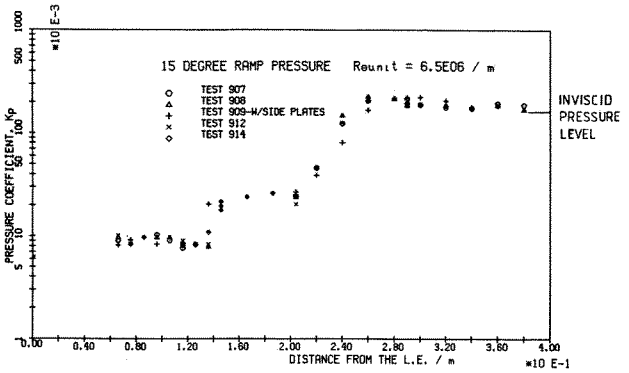

(a) 15° ramp deflection angle

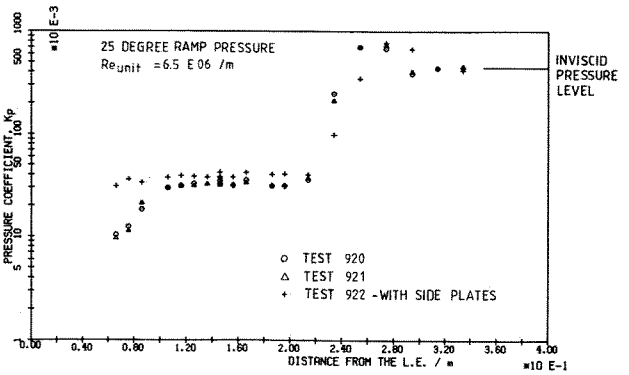

(b) 25° ramp deflection angle

Fig. 9 - Pressure distribution over the flat plate/2D ramp model - repeatability and effect of side plates

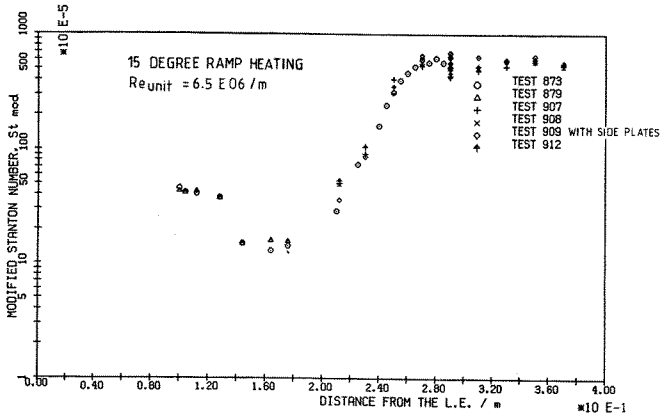

(a) 15° ramp deflection angle

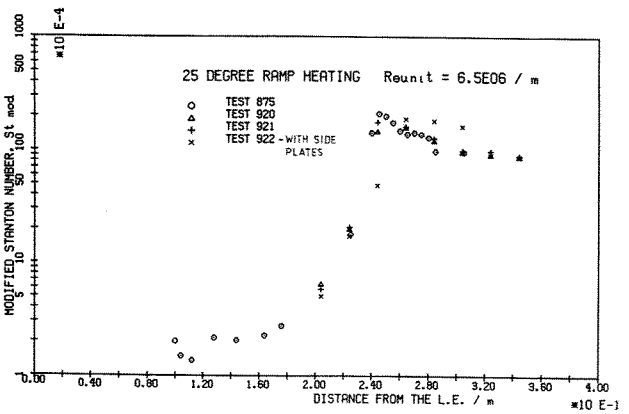

(b) 25° ramp deflection angle

Fig. 10 - Heat transfer distribution over the flat plate/2D ramp model - repeatability and effect of side plates

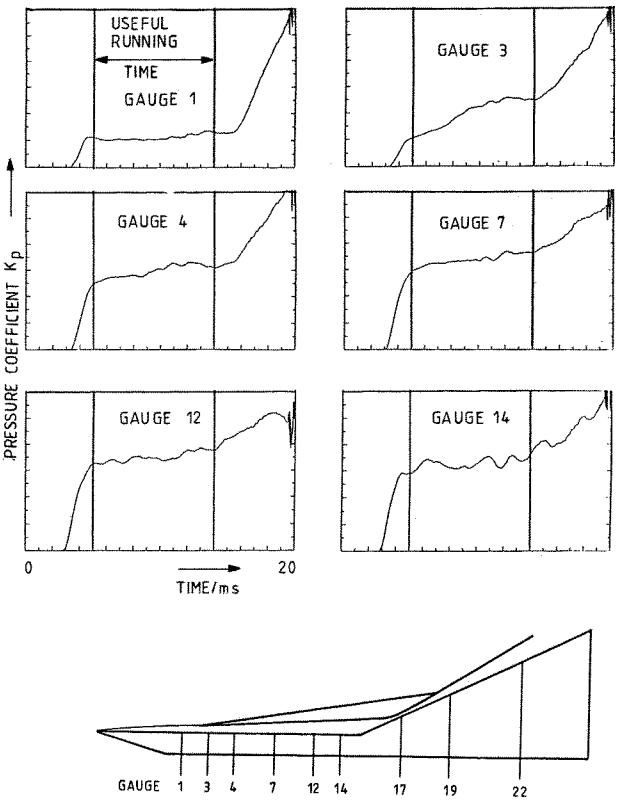

Fig. 11 - Pressure coefficient time traces on the flat plate part of 25° ramp model

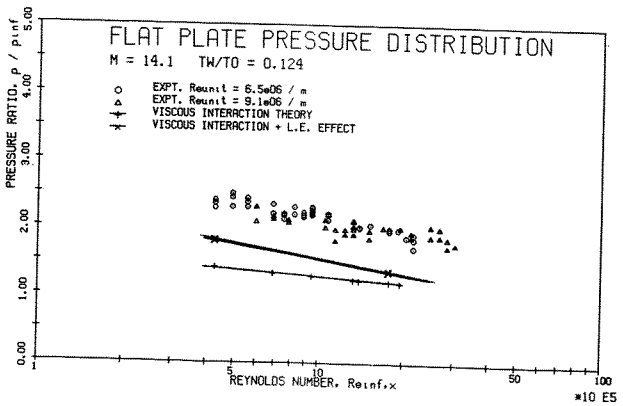

Fig. 12 - Pressure distribution over the flat plate model - comparison with wall viscous interaction and inviscid leading edge bluntness theories

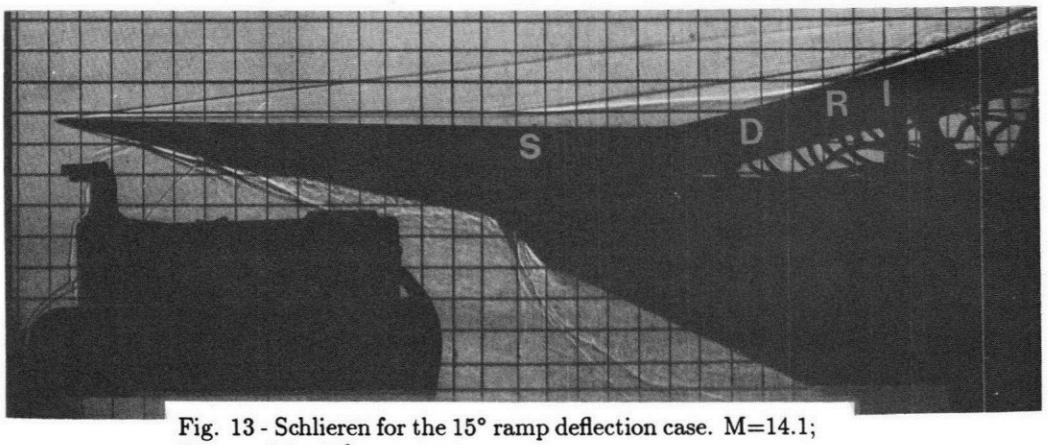

Fig. 13 - Schlieren for the 15° ramp deflection case. M=14.1; Re_{unit}=6.5×10^6 per meter

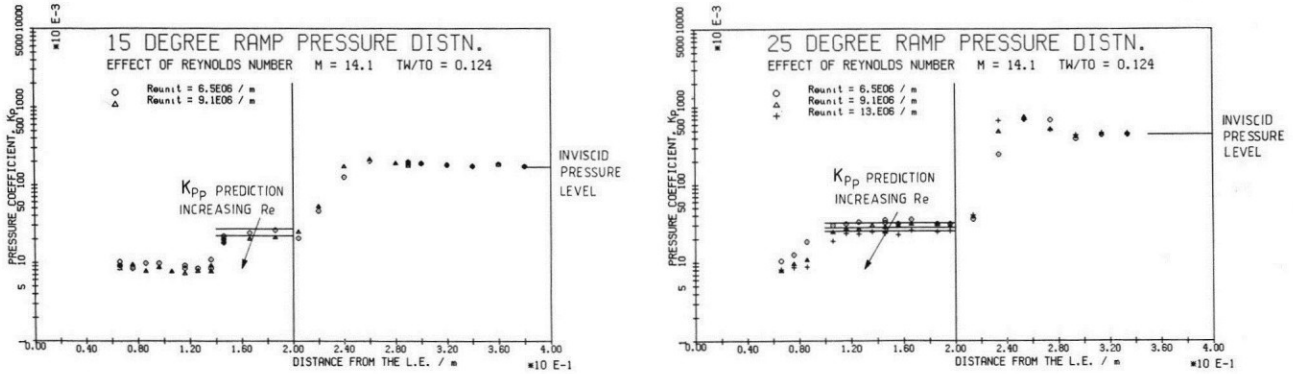

(a) 15° ramp deflection angle

(b) 25° ramp deflection angle

Fig. 14 - Effect of Reynolds number on the pressure distribution over the flat plate/2D ramp configurations

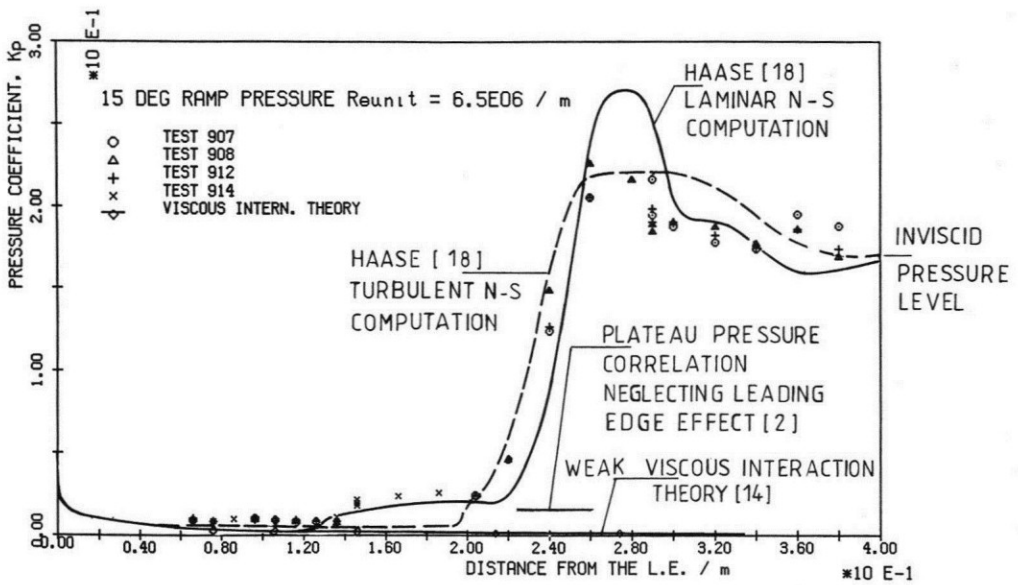

Fig. 15 - Comparison of the pressure distribution over the 15° ramp configuration to the Navier-Stokes computation of Haase

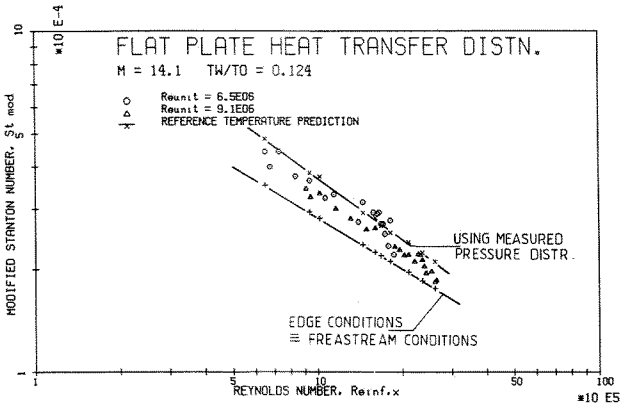

Fig. 16 - Heat transfer distribution over the flat plate configuration - comparison with Eckert's reference temperature prediction method

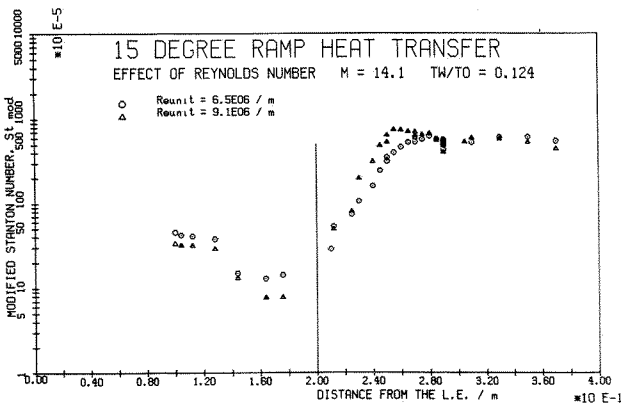

(a) 15° ramp deflection angle

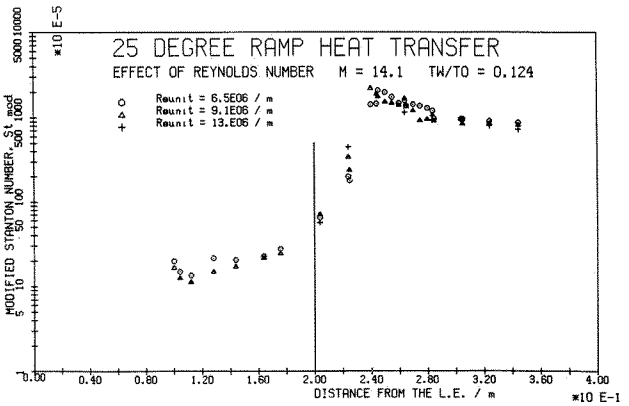

(b) 25° ramp deflection angle

Fig. 17 - Effect of Reynolds number on the heat transfer distribution over the flat plate/2D ramp configurations

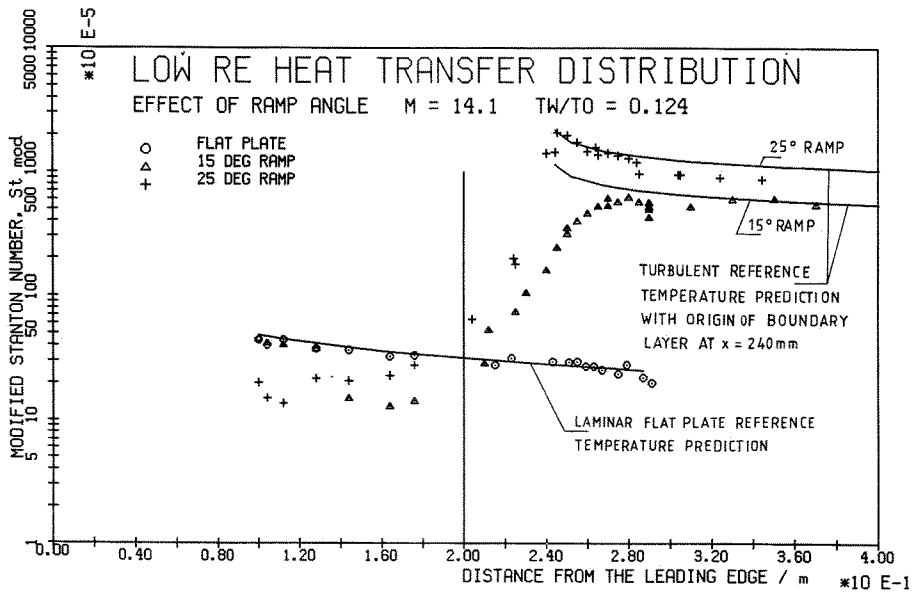

Fig. 18 - Effect of ramp angle on the heat transfer distribution over the flat plate/2D ramp configuration and comparison to local edge conditions flat plate theory

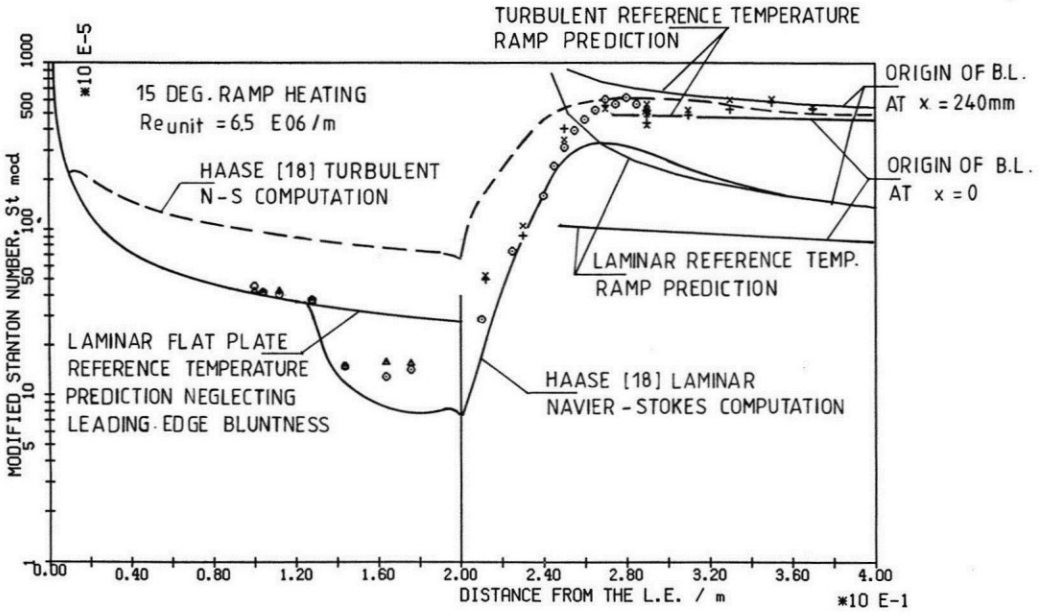

Fig. 19 - Comparison of heat transfer distribution over the 15° ramp configuration to the Navier-Stokes computation of Haase

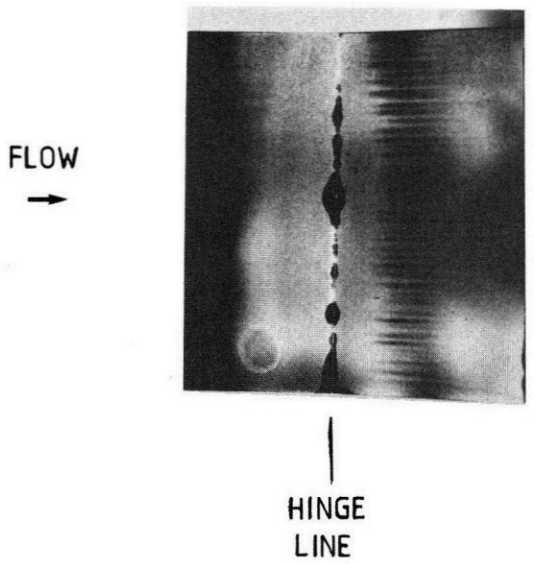

Fig. 20 - Sublimation visualization over a flat plate/2D 15° ramp model at Mach 6

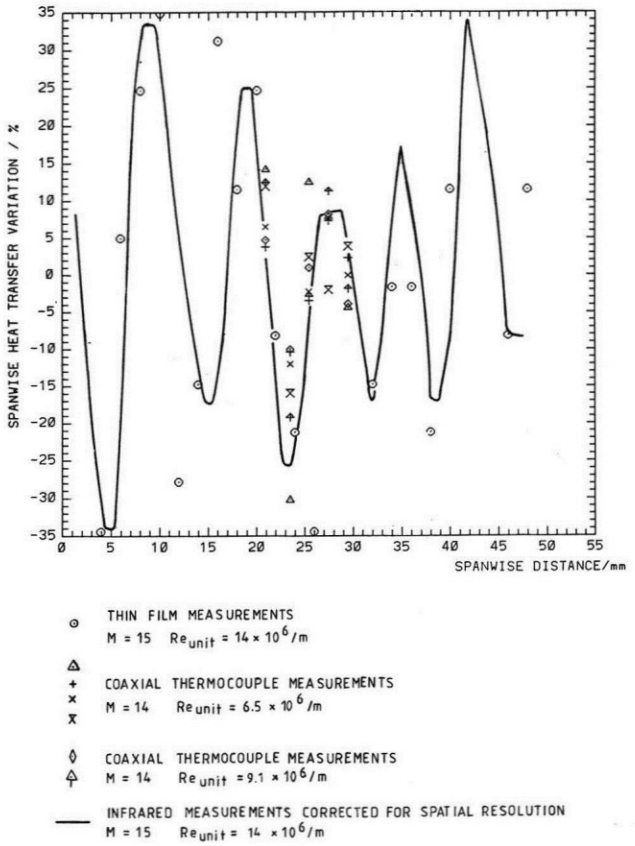

Fig. 21 - Spanwise heat transfer variation near reattachment on the flat plate/2D 15° ramp configuration